# Preparation Studies for Secondary Electron Emission Experiments on Superconducting Niobium

Anoop George and Robert A. Schill, Jr.
Department of Electrical and Computer Engineering
University of Nevada, Las Vegas
4505 Maryland Parkway
Las Vegas, Nevada 89145-4026
anoopg@egr.unlv.edu

March 7, 2004

# Preparation Studies for Secondary Electron Emission Experiments on Superconducting Niobium

*Anoop George* and Robert A. Schill, Jr.
Department of Electrical and Computer Engineering
University of Nevada, Las Vegas
4505 Maryland Parkway
Las Vegas, Nevada 89145-4026
anoopg@egr.unlv.edu

*Abstract*

Accelerator driven transmutation of waste is one complementary approach to deal with spent nuclear fuel as compared to permanent storage. High-energy protons generated by a particle accelerator collide with a heavy metal target producing neutrons. Long-lived radioactive isotopes interacting with the neutrons transmute into shorter-lived isotopes. To generate the high-energy protons efficiently, linear accelerators use multi-cell superconducting radio frequency (RF) cavities made of niobium. Superconducting niobium cavities have several advantages, including small power dissipation. The high electromagnetic fields present in these cavities may result in undesired field emission from surface imperfections with the probability of generating an avalanche of secondary electrons from a localized resonant process of impacting known as multipacting. Undesirably, this localized electron current absorbs the RF power supplied to the cavity. This in turn leads to an increase in cavity wall temperature and the eventual breakdown of the wall's superconductivity. In addition, this can result in structural damage to the cavity surface and the degradation of cavity vacuum. As a result, the $Q_0$ (quality factor) of the cavity is significantly reduced. A good cavity design should be able to eliminate, or at least minimize multipacting. The factors that affect multipacting include shape, surface finish and conditioning, and the secondary electron yield of the material.

It is desired to measure the distributed secondary electron yield from a Los Alamos National Laboratory surface prepared niobium test piece in the superconducting state under ultra high vacuum (UHV). A micro-channel plate/delay-line-anode detector (MCP/DLD) capable of single particle position and timing will be used to determine, with the aid of particle tracking codes, the secondary electron yield. The experimental setup primarily evolves around the detector to measure the secondary electron beam and the physics to be studied.

Simulation studies using an electromagnetic particle tracking code will be presented to establish the system parameters and geometry, and examine constraints and resolutions of the experimental setup. With the aid of a biasing grid, secondary electrons with 1 eV increments in initial energies between 1 and 20 eV for a wide range of launch angles can be captured and distinguished on a 4.5 cm diameter MCP/DLD detector. An experimental setup is presented.

## I. INTRODUCTION

Multipacting is a serious issue in the design of accelerators for accelerator driven transmutation of waste. Multipacting is a localized resonant current resulting from multiple impacts leading to an avalanche build up of secondary electrons. This oscillating surge of current limits the amount of energy that can be stored in the accelerator cavities. At Los Alamos National Laboratory (LANL), multipacting is a concern in the multi-cell superconducting RF cavity. [1,2] A good cavity design should be able to eliminate, or at least minimize multipacting. The factors that affect multipacting include the shape, surface finish and coating, and the secondary electron yield of the material.

It is desired to measure the distributed secondary electron yield from a niobium sample under conditions that closely emulate the environment of the superconducting RF linear accelerator at LANL. The measured secondary electron yields from, LANL specific, surface conditioned niobium samples will be incorporated in cavity design codes that examine mulitipacting effects. To this end, the experiment will be conducted in a $10^{-7}$ Pa ($10^{-9}$ Torr) ultra high vacuum (UHV) environment at cryogenic temperatures in a niobium superconducting state (< 8.5 $^{o}$K) [3]. The experimental setup is dictated by the physics sought and primarily the secondary electron detector. Other considerations such as the electron gun, the sample shape, mounting and positioning logistics, cryogenic techniques and other peripheral sensors will not be considered here. Calculations and simulations presented suggest an optimized geometry for the experimental setup based on the physics to be examined. Further, simulations suggest the type and parameters of detector required. Spatial and temporal resolution calculations suggest that scintillating photomultiplier and the low energy electron diffraction (LEED) type detectors are not sufficient for distribution studies of the secondary electrons [4]. The choice of the detector constrains the electron gun parameters and the configuration of the experimental setup. A specially designed micro-channel plate/delay-line-anode (MCP/DLD) detector, with a $250\mu m$ spatial resolution and a multi-hit capability of detecting 4 particles in 10 ns, has been chosen for single particle position and timing detection. With the aid of particle tracking codes, the initial particle trajectory parameters of the emitted secondary electron can be determined.

## II. ANALYTICAL STUDIES

Based on a typical secondary electron energy range, an estimate for the spatial resolution of the detector is determined. For simplicity in this first order calculation, all fringe effects due to the finite detector with aperture opening and the hemispherical niobium target are neglected. Consequently, the hemispherical niobium target is assumed to be a grounded sphere with radius $R_1$. The finite geometry detector is assumed to be a spherical shell of radius $R_2$ at potential $V_s$. The two spherical components are concentric allowing for a high degree of symmetry. This symmetry allows the orientation and finite geometry of the detector to not influence the orbit trajectory of a particle launched from any point on the niobium surface. In practice, a spherical shell detector is expensive and difficult to build. If the distance of separation between the detector and the niobium target is small and the emitted particle remains centrally located both

relative to the finiteness of the two components, the difference between the real and approximated particle orbit trajectories will be small.

Consider that a primary electron launched from an electron gun passes through a small hole in the detector and strikes the niobium target on the primary beam axis. The z-axis of a coordinate system with origin located at the concentric center of the spheres is oriented along the beam axis. The governing equations of motion, in spherical coordinates, for a charge emitted from the niobium surface on the z-axis are

$$\ddot{r} - r\dot{\theta}^2 - r\dot{\phi}^2 \sin^2\theta = K/r^2 \tag{1}$$

$$2\dot{r}\dot{\theta} + r\ddot{\theta} - r\dot{\phi}^2 \sin\theta\cos\theta = 0 \tag{2}$$

$$2\dot{r}\dot{\phi}\sin\theta + 2r\dot{\theta}\dot{\phi}\cos\theta + r\ddot{\phi}\sin\theta = 0 \tag{3}$$

where the electric field, as obtained from Gauss' law, between the spherical equipotential surfaces is

$$\vec{E}(r(t)) = \hat{r}\frac{V_S}{r^2(t)}\left[\frac{R_1R_2}{R_2 - R_1}\right] = \hat{r}\frac{mK}{qr^2(t)} \tag{4}$$

where q and m are respectively the charge and mass of the emitted secondary electron.

A secondary electron emitted from the niobium surface on the z-axis exhibits no azimuthal motion implying that $\ddot{\phi} = \dot{\phi} = 0$. Consequently, Eqs. (1) and (2), simplify as

$$\ddot{r} - r\dot{\theta}^2 = K/r^2 \tag{5}$$

$$2\dot{r}\dot{\theta} + r\ddot{\theta} = 0 \tag{6}$$

Multiplying Eq. (6) by $\dot{\theta}$ and simplifying yields

$$C_0 = r\dot{\theta}/2 \tag{7}$$

where $C_0$ is a constant of motion. This constant is determined from the energy conservation relation

$$\frac{1}{2}mv^2 + qV(r) = \mathrm{E}_0 \tag{8}$$

where $\mathrm{E}_0$ is the initial energy of the particle just after it is emitted from the niobium surface and v is the velocity in spherical coordinates given by

$$v^2(t) = \dot{r}^2 + \left(r\dot{\theta}\right)^2 \tag{9}$$

Using Eqs. (7)-(9), $C_0$ can be expressed as

$$C_0 = \left[ \frac{\mathrm{E}_0 - 0.5 m v_{ro}^2}{2m} \right]^{1/2} \tag{10}$$

where $v_{ro}$ is the initial radial velocity of the emitted electron. With the aid of Eq. (7), Eq. (5), simplifies to

$$\ddot{r} = \frac{K}{r^2} + \frac{4C_0^{\,2}}{r} \tag{11}$$

The source voltage range is fixed by the limits of the detector, $0 \le V_S \le 1kV$. Further, based on well-known scanning electron microscopy literature [5] and solid state physics [6,7], typical secondary electron energies lie within the range of 1eV and 50 eV. There remain a large number of parameters to be considered. Consequently, Eq. (11) is not in an optimized form suitable for computation. Therefore, the following normalization is introduced: $r = \tilde{r} R_2$, $\mathrm{E}_0 = \tilde{\mathrm{E}}_0 q V_s$, $R_1 = \tilde{R}_1 R_2$, $v_{ro} = \tilde{v}_{ro} [2qV_s/m]^{1/2}$ and $t = \tilde{t} R_2 [m/(qV_s)]^{1/2}$. The normalized Eqs. (11) and (7), with the associated constants given by Eqs. (4) and (10), are respectively,

$$\frac{d^2\tilde{r}}{d\tilde{t}^{\,2}} = \frac{\tilde{R}_1}{\tilde{r}^{\,2}\left(\tilde{R}_1 + 1\right)} + 2\frac{\tilde{\mathrm{E}}_o - \tilde{v}_{ro}^2}{\tilde{r}} \tag{12}$$

$$\frac{d\theta}{d\tilde{t}} = \frac{\left[2\left(\tilde{\mathrm{E}}_o - \tilde{v}_{ro}^2\right)\right]^{1/2}}{\tilde{r}} \tag{13}$$

Figure 1 corresponds to $\tilde{R}_1$ family of curves yielding the normalized radial position $\tilde{r}$ of a charge at normalized time $\tilde{t}$ for an initial normalized energy of 0.001 and zero initial motion along the z-axis. When $\tilde{r} = 1$, the electron has reached the surface of the detector. Therefore, the intersection of the family of curves displayed with the $\tilde{r} = 1$ line yields the normalized time it takes for the electron to reach the detector surface.

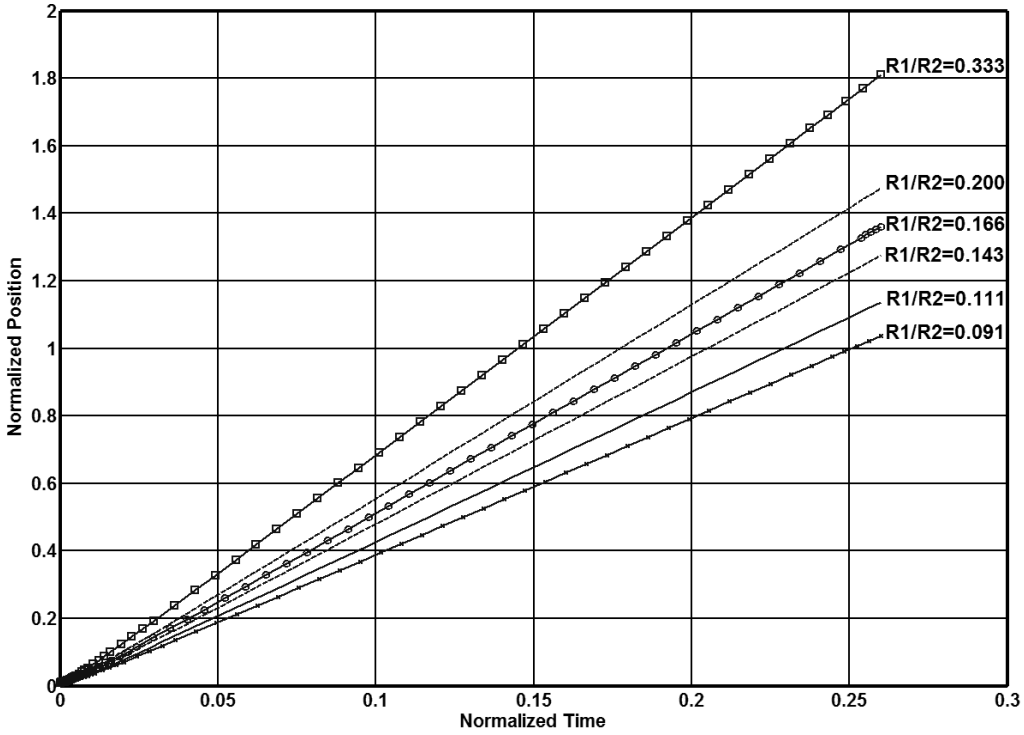


Fig. 1. Displays the normalized radial position of the particle $\widetilde{r}$ with respect to the normalized time $\widetilde{t}$ when the initial motion along the z-axis is zero for various $\widetilde{R}_1$ when $\widetilde{\mathrm{E}}_0 = 0.001$.

The change in the conical angle of the particle trajectory is estimated as

$$d\theta / d\widetilde{t} \approx \theta / \widetilde{t} \tag{14}$$

The difference in the conical angle between any two different energetic electrons may be translated into normalized distance $\Delta\widetilde{D} = \Delta D / R_2$ on the spherical detector between two electron impact points contained in an azimuthal plane as

$$\Delta\widetilde{D} = (\theta_2 - \theta_1) \tag{15}$$

where $\theta_1$ and $\theta_2$ are the conical angles of the two impact points relative to the z-axis. Further, the normalized distance projected onto a flat screen normal to the the z-axis is

$$\Delta\widetilde{D}_{flat} = \cos\theta_1 \left(\tan\theta_2 - \tan\theta_1\right) \tag{16}$$

The normalized time for a 1 eV electron to impact the detector may be obtained from Fig. 1. For $\widetilde{R}_1 = 0.166$, $\widetilde{\mathrm{t}} = 0.19204$. For 20 eV electrons [simulations not shown], $\widetilde{\mathrm{t}} = 0.19180$. The normalized time interval, $\Delta\widetilde{t}_T$, between the 1 eV and 20 eV impacts is the difference between the

times, $\Delta\tilde{t}_T = 0.00024$. For a $\tilde{R}_1 = 0.091$, $\Delta\tilde{t}_T = 0.0021$ (20 eV simulations not shown). For each eV increment in energy, the normalized time interval, $\Delta\tilde{t}_p$, is approximately constant over this energy spread. Therefore, $\Delta\tilde{t}_p = \Delta\tilde{t}_T / 20$. The normalized time interval may be determined for any electron energy in this range. The normalized overall arc length dimension of the detector, $\tilde{D}_T = 2\Delta\tilde{D}$, to collect secondary electrons with energies between 0 eV to some maximum value is determined using the computed normalized time and Eqs. (13)-(15) with $\tilde{r} = 1$, $\theta_1$=0 and $\theta_2 = \theta_{\max}$. Consequently, if all secondary electrons with energies between 0 eV and 20 eV are to be collected assuming a 0.5 cm radius sample, then, for $\tilde{R}_1 = 0.166$ and a detector radius of 3 cm the arc length of the detector, D, is 2 mm. If it is desired to resolve the electron energy in integer increments of eV, then, the normalized time interval between a 1 eV and 2 eV electron is $\Delta\tilde{t}_p = 0.000012$, based on $\tilde{t}$ for $\tilde{R}_1 = 0.166$. From Eqs. (13) and (14), the conical angle for the 1 eV and 2 eV particles are $\theta_1 = 8.56$ mrad and $\theta_2 = 12.1$ mrad. The resolution given by Eq. (16) is 90 μm. For a potential difference of 200 V, a 0.5 sample radius and a 3 cm detector radius of curvature, the overall arc length of the detector is 5 mm and the resolution 200 μm. When projected onto a flat screen, the corresponding detector diameter and spatial resolution required were found to be approximately the same.

## III. SIMULATION STUDIES

A number of computer simulations using a particle tracking code, developed by Field Precision Inc., were performed over a wide parameter space. The purpose of the simulations was to establish a more accurate study of the detector size, resolution, and a more realistic experimental geometry setup. The loading effects of the finite geometries of a planar MCP/DLD detector with posts, cryostat configurations, electron gun, and other conducting and non-conducting surface were incorporated in the simulations. A grid near the detector surface and an electron beam drift tube between the detector and gun allows for the control of the spatial resolution on the detector and niobium surfaces respectively. Only six simulations that established the experimental setup will be presented.

Figure 2 corresponds to a 1 eV secondary electron generated due to the primary electron beam impinging normal to the hemispherical niobium surface. A 1 cm diameter hemispherical niobium sample lies on a 2.5 cm diameter cryostat cylinder. The top surface of the sample is 2.5 cm from a grid mounted 3 mm in from of the front face of the MCP/DLD detector. The oblique incident case is a consequence of the sample with cryostat displaced 4mm horizontally from the primary electron beam axis. An electron beam drift tube with a 3 mm outer diameter and a 2 mm inner diameter coated with a 0.5 mm layer of VESPEL insulation is mounted in a 6 mm diameter central aperture in the detector. As shown at the top of the figure, the drift tube is inserted in the electron gun aperture. The electron beam tube, electron gun casing, the cryostat and the niobium sample are held at ground potential. Although not considered, the vacuum chamber is also at ground potential. The MCP/DLD consists of a chevron stack of two MCPs and resistive anode wires. The front face of the MCP (surface facing the grid) must be at a potential of 200 V above

the grid. For maximum gain the back face of the first MCP must be 1400 volts above the MCP's front face. The back face of the second MCP must be at a potential of 1400 V above the back face of the first MCP. Finally the anode wires must be at least 200 volts above the back face of the second MCP. The voltage of the anode wires is 3000 V above the grid potential.

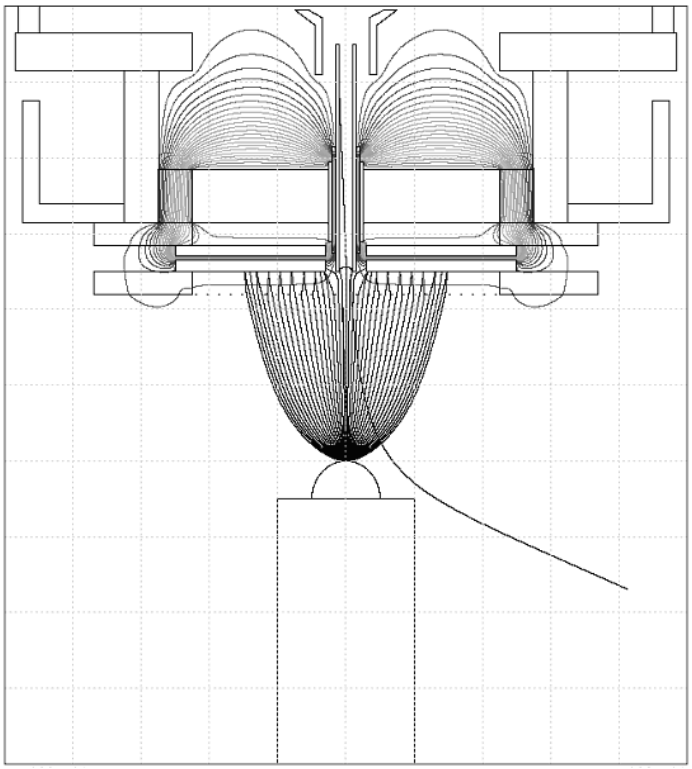

Fig. 2. Trajectories of 1 eV secondary electrons with different launch angles, for coincident sample and primary beam axes (normally incident primary electron beam)

As shown in Fig. 2 the particle trajectory orbit was followed for initial angles of projection between $0^o$ and $180^o$ in $4.5^o$ increments. This corresponds to 41 particles being launched in each case. All angles are measured with respect to the plane tangent to the niobium surface at the point of primary electron beam impact. It is observed that between 17 % and 12 % of the total number of particles are lost in the aperture opening for particle energies between 1 eV and 20 eV respectively. The percentage of particle loss due to the finite dimension of the detector, for particle energies between 1 eV and 20 eV, is 0% and 38% respectively. Table 1 provides the range of initial projection angles captured or lost in the detection process for particles of different energy and of different incidence. Typically, the energy distribution of emitted secondary electrons occurs between 2 eV and 3 eV. The spatial resolution of the MCP/DLD detector is 250 μm. Based on this resolution, the detector can resolve 1 eV increments in energy and $4.5^o$ increments in initial angle of projection between $0^o$ to $70^o$ and $110^o$ to $180^o$. For oblique incidence ($60^o$ to the surface normal), the grid potential had to be increased to 800 V in order to collect 100% and 54% of 1 eV and 20 eV secondary electrons launched respectively.

Table 1. Simulation outcome for detector size, detector resolution and experimental setup leading to a final experimental design.

| Incidence | Grid Voltage [V] | Secondary Electron Energy [eV] | Initial Angle of Projection Electrons Collected $\theta_{min} \le \theta \le \theta_{max}$ | Initial Angle of Projection Electrons Lost to Aperture $\theta_{min} \le \theta \le \theta_{max}$ | Initial Angle of Projection Electrons Lost Due to Detector Size $\theta_{min} \le \theta \le \theta_{max}$ | *Smallest / Average Detector Resolution [$\mu$m] |
|---|---|---|---|---|---|---|
| Normal | 25 | 1 | $0^o$-$75^0$ and $105^o$ -$180^0$ | $75^o$-$105^o$ | none | ~50/ 700 |
| Normal | 25 | 2 | $0^o$-$75^0$ and $105^o$ -$180^0$ | $75^o$-$105^o$ | none | ~200/1100 |
| Normal | 25 | 20 | $35^o$-$80^o$ and $100^o$-$145^o$ | $80^o$-$100^o$ | $0^o$-$35^o$ and $145^o$ -$180^o$ | 1700/2200 |
| Oblique | 800 | 1 | $0^o$-$180^0$ | none | none | 50/200 |
| Oblique | 800 | 2 | $0^o$-$165^0$ | $165^o$-$180^o$ | none | 100/300 |
| Oblique | 800 | 20 | $55^o$-$140^o$ and $170^o$-$180^o$ | $140^o$-$170^o$ | $0^o$-$55^o$ | 600/1100 |

* Smallest distance between two equal energy particles with a $4.5^o$ difference in initial angle of projection.

## IV. CONCLUSION

Analytical studies on the secondary electron motion were performed which provided a reasonable range of detector sizes, detector resolutions and distances from sample to detector. Particle tracking simulations provided a complementary in-depth study of these parameters. It was determined that a 4.5 cm diameter detector with 250 $\mu m$ resolution positioned 2.5 cm from the sample allows for an optimal collection of secondary electrons in a 10" diameter vacuum chamber.

REFERENCES


[1] A Roadmap for Developing Accelerator Transmuting of Waste (ATW) Technology. DOE/RW-0519, 1999.

[2] Padamasee, Hassan, J. Knobloch, T. Hays. RF Superconductivity for Accelerators. New York: John Wiley, 1998. 454.

[3] Cook, Zemansky and Boorse. "The Superconductivity of Columbium." Physics Review 80 (1950): 737.

[4] Oelsner, A."Micro spectroscopy and imaging using a Delay line Detector in time-of-flight photoemission microscopy." Review of Scientific Instruments 72 (2001).

[5] Reimer, Ludwig. Scanning Electron Microscopy: Physics of Image Formation and Microanalysis. New York: Springer Verlag, 1998.
[6] Dekker, Adrianus J. Solid State Physics. New Jersey: Prentice Hall, 1957. 419.
[7] Hachenberg, O. and W. Brauer. "Secondary Electron Emission from Solids." Advances in Electronics and Electron Physics 11 (1959): 413-499.